

Particle and Plutonium Mobilization in Macroporous Soils during Rainfall Simulations

J. N. RYAN,^{*,†} T. H. ILLANGASEKARE,[†]
M. I. LITAOR,[‡] AND R. SHANNON[§]

Civil, Environmental, and Architectural Engineering
Department, University of Colorado, Campus Box 428,
Boulder, Colorado 80309, Department of Biotechnology and
Environmental Sciences, Tel-Hai Rodman College, Upper
Galilee, 12210, Israel, and Paragon Analytics, Inc.,
Fort Collins, Colorado 80524

To test the effects of infiltration velocity, soil type, and soil structure on the mobilization of particles in the unsaturated zone, we monitored particle concentrations and plutonium activities in water moving through macroporous soils during rainfall simulations at the Rocky Flats Plant in Colorado. Rainfall simulations were conducted in three soil pits at the same intensity and in one soil pit at three intensities. The rapid arrival of water at zero-tension samplers located at depths from 15 to 70 cm indicated that macropore flow dominated infiltration. Most of the particle mobilization occurred during the initially slow infiltration of the first small volumes of rainfall to pass through the soil, resulting in a lack of correlation between particle concentration and the discharge rate (Darcy velocity) of the infiltrating water. Particle size distributions (1–50 μm) were steady during the simulations and displayed greater mass in the larger size ranges. The amount of particle mobilization was not related to soil composition. Three successive applications of rainfall over 5–10-day intervals to the same soil pit depleted the supply of particles that could be mobilized. The plutonium content of the particles decreased with depth, and plutonium transport was largely attenuated in the upper 15–20 cm of soil.

Introduction

The infiltration of many contaminants through the unsaturated zone is accelerated by association with mobile particles (1, 2). To predict the rate of infiltration of these contaminants, we must focus our attention on the mobilization and transport of soil particles. Particles mobilized during rainfall infiltration include clay minerals, sesquioxides, quartz and feldspar fragments, and organic matter coatings in colloidal to silt size ranges at concentrations as high as 1.7 g L^{-1} (3–5).

Soil scientists have long recognized that particles are “translocated” or “illuviated” to lower soil horizons (6, 7), but little is known about the rate of particle mobilization or its dependence on rainfall intensity. Soil particles may be mobilized by both chemical and physical perturbations (8)—the low ionic strength of rainfall increases electrostatic repulsion between particles and grains and the infiltrating

water imposes shear stress on particles—but because rainfall chemistry is fairly constant, variations in rainfall intensity are expected to affect particle mobilization most significantly.

In model systems consisting of fluids flowing over spherical particles attached to flat surfaces, the hydrodynamic shear force F_{shear} depends on the flow velocity U_f at the center of the particle, the fluid viscosity μ , and the particle radius r (9):

$$F_{\text{shear}} = 1.7009(6\pi)\mu r U_f \quad (1)$$

The shear force is opposed by a net electrostatic attractive force that binds the particles to the grain. If the hydrodynamic shear force exceeds the attractive force, the particle will be mobilized (10). On the basis of eq 1, an increase in velocity will increase the shear force and, hence, the amount of particles mobilized. An increase in particle size will also increase the shear force. In addition, a decrease in the attractive force caused by chemical perturbation will promote particle mobilization.

Testing this relationship in real soils is difficult owing to initially unsaturated conditions and heterogeneity of soil composition and particle size. In accordance with shear theory, Kaplan et al. (4) reported that the amount of particles mobilized was directly related to the flow rate of free-flowing soil water in a soil repacked into a large test chamber. Kaplan et al. (4) also reported that the size of mobilized particles increased as the rate of infiltration increased, a result at odds with shear theory. Biddle et al. (5) reported no correlation between rainfall intensity and colloid mobility in samples removed by suction during natural rainfall experiments under in situ conditions. A further complication involves the role that soil structure may play in particle mobilization. Macropores formed by desiccation, root decay, and earthworm burrowing have been linked to enhanced infiltration of water, solutes (11), bacteria (12), particles (3, 13), and particle-associated actinides (14), but their effect on particle mobilization has not been examined.

To test the effect of rainfall intensity, soil type, and soil structure on particle mobilization, we conducted in situ rainfall simulations at the Rocky Flats Plant, a former nuclear weapons manufacturing facility located about 20 km northwest of Denver, CO. The soils are contaminated by actinides that associate strongly with particles (Pu, Am, and U) and marked by macropores formed by earthworm burrowing and root decay that extend to depths of 30–100 cm (14–16). These field tests extend our understanding of particle mobilization in soils by (a) combining controlled rainfall simulations with monitoring of particle mobilization under in situ conditions, (b) examining the transport of a wide size range of soil particles, and (c) focusing on the role of macropores in particle mobilization and transport.

Materials and Methods

Site Description. The rainfall simulations were conducted during August 1993 on a grassy hill slope near a former storage site of steel drums that contained plutonium-contaminated industrial oils (Figure 1). From 1958 to 1968, about 100 g of plutonium leaked from the drums, attached to soil particles, and was blown east and southeast by the prevailing winds (15, 17). The fine-loamy, mixed, mesic Aridic Argiustoll soils contain three major horizons—organic-rich A, clay-rich upper B, and calcified lower B (Table 1; Figure 2). The soils contain macropores formed by decayed root channels and earthworm burrows of $>1 \text{ mm}$ width that extend to depths of 30–100 cm. The fillings of these macropores contain significantly

* Corresponding author phone: 303-492-0772; fax: 303-492-7317; e-mail: joe.ryan@colorado.edu.

[†] University of Colorado.

[‡] Tel-Hai Rodman College.

[§] Paragon Analytics, Inc.

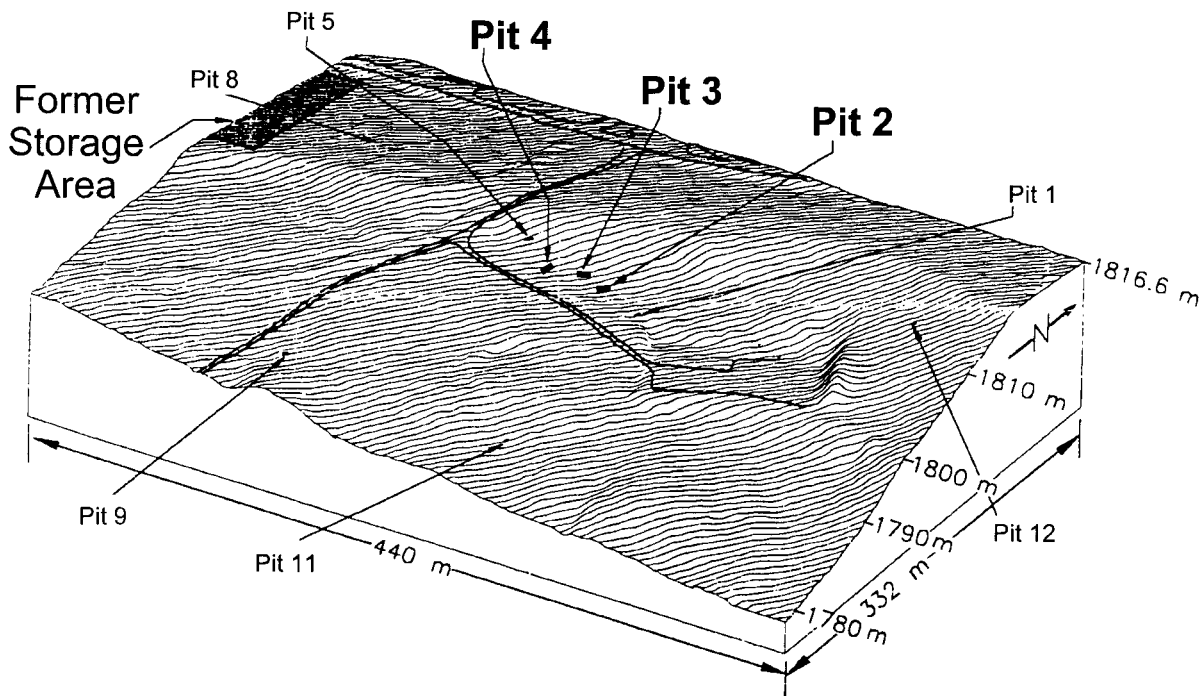


FIGURE 1. Block diagram of study site near former storage area of drums containing plutonium-contaminated oils. Soil pits 2–4 used in this study; other pits used in previous studies (16).

TABLE 1. Physical, Chemical, and Mineralogic Characteristics of Soil Horizons Present in Soil Pits 2–4 at the Rocky Flats Plant (15, 20)

soil pit	soil horizon	depth (cm)	sand ^a (%)	silt ^a (%)	clay ^a (%)	sesquioxides ^b (mmol kg ⁻¹)	CaCO ₃ (mmol kg ⁻¹)	CEC (mmol kg ⁻¹)	organic carbon (g kg ⁻¹)	pH	smectite ^c (%)
2	A	0–7	64.4	19.1	16.5	98	40	274	100	7.2	5–30
	Bw	7–19	69.8	15.3	14.9	92	30	198	54	7.0	5–30
	Bt	19–50	49.1	16.7	34.2	72	20	228	13	7.0	30–60
	2Bt	50–105	36.1	27.4	36.5	136	50	198	6	7.0	30–60
	3BCgk1	105+	14.1	40.9	45	52	270	265	2	7.5	>60
3	A	0–18	67.3	17.1	15.6	94	100	279	100	7.0	5–30
	AB	18–35	58.1	15.6	26.3	155	40	233	20	7.1	30–60
	Bw	35–51	60.4	13.9	25.7	178	20	208	39	7.0	30–60
	BC	51–120	16.0	44.1	39.9	203	10	296	3	7.7	>60
	BCK1	120+	22.4	43.6	34.0	64	350	260	2	7.8	>60
4	A	0–18	64.1	18.6	17.3	95	60	241	160	6.7	5–30
	Bt1	18–41	38.4	21.6	40.0	171	40	279	18	6.5	5–30
	Bt2	41–77	37.9	23.6	38.5	143	10	197	6	7.5	30–60
	BCg	77–108	38.6	23.9	37.5	245	90	264	9	7.3	30–60
	2BCg	108+	24.4	37.2	38.4	75	40	264	4	7.8	>60

^a The sand, silt, and clay size fractions are >50, 2–50, and <2 μm, respectively. ^b Sesquioxide content is sum of Fe, Mn, and Al measured in dithionite–citrate–bicarbonate soil extracts. ^c Smectite content is listed as the abundance of the clay size fraction.

greater plutonium activity than the surrounding soil, indicating that they are pathways for preferential transport (15). The average water table below the pits is located at depths of 1.5–2.5 m; hence, the macropores do not reach the water table.

Sampling Pits. The rainfall simulations were conducted adjacent to three soil pits (pits 2–4) excavated and instrumented by Litaor et al. (16) about 1 year before these experiments. Free-flowing water was sampled from zero-tension samplers (ZTSs) in each pit to examine the effect of macropores on particle mobilization. The ZTSs were installed where macropores (>1 mm width) were evident. Water flowing into the ZTSs drained into bottles in the base of each pit and was pumped to the surface using a vacuum pump.

Rainfall Application. The simulations were conducted by applying water over the upslope side of the pits following the schedule in Table 2. The 8.3 cm h⁻¹ rainfall rate

approximately represents the rainfall intensity of the 100-year return event for this area (7.7 cm h⁻¹) (16). The rainfall was delivered by a triple-nozzle sprayer that traveled back and forth across a 6 m × 1 m area at a rate of about 6 m min⁻¹. The test areas were surrounded by a polyethylene wind skirt to minimize water loss. The fine sprays of water delivered by the nozzles did not properly simulate the impact of raindrops; however, the nozzles did ensure even distribution of the rainfall, which was checked using three rain gauges in the wetted area. Tap water was used as rainfall for these experiments. The specific conductance of the tap water (30 μS cm⁻¹) was higher than that of precipitation in this area (5–10 μS cm⁻¹) but still much lower than that of the soil water (200–500 μS cm⁻¹); therefore, the difference in ionic strength between the tap water and precipitation should not have affected the extent of particle mobilization.

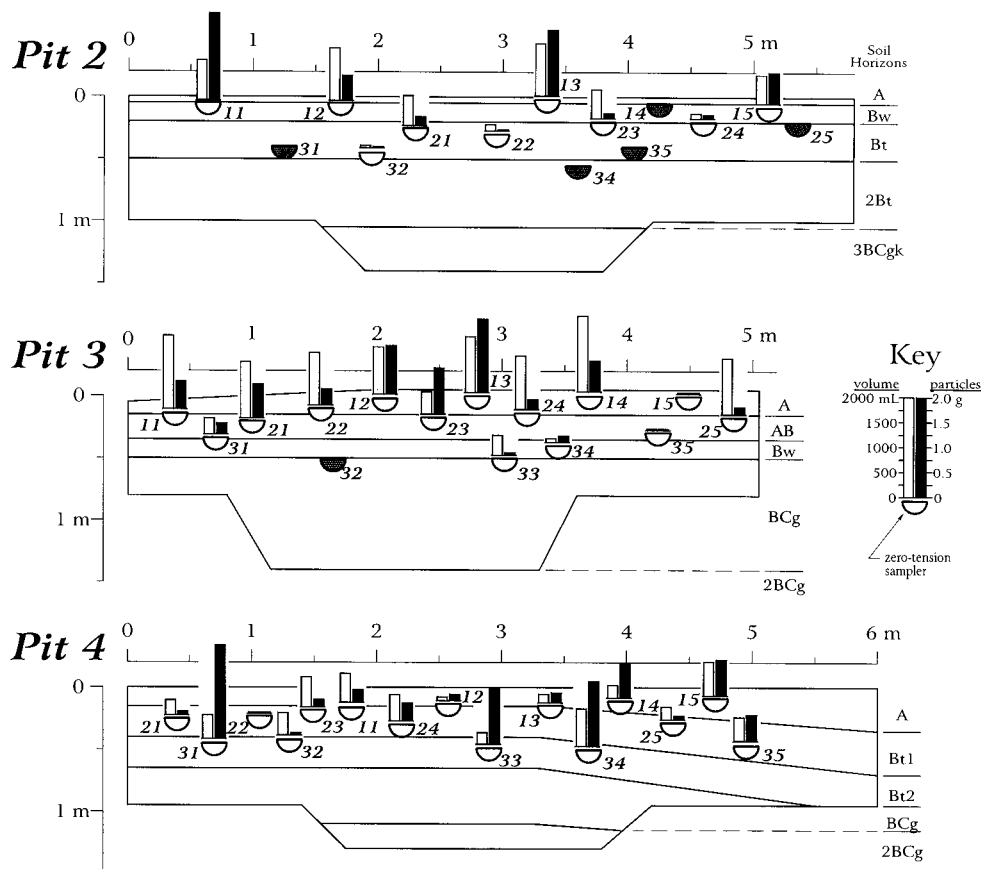


FIGURE 2. Cross-sections of soil pits used for rainfall simulations show dimensions, soil horizons, and total particle mass and water volumes arriving in each zero-tension sampler (ZTS) during the 8.3 cm h^{-1} simulations. Infiltrating water was never recovered from the darkened ZTSs (e.g., ZTS 31 in pit 2). ZTS collection bottles were buried in the center depressions in each pit.

TABLE 2. Schedule of Rainfall Simulations at the Rocky Flats Plant during August 1993

date (1993)	soil pit	rainfall rate ^a (cm h^{-1})	vol (L)	time (h)	no. of samples
August 3	pit 2	8.3	500	1.0	64
August 4	pit 3	8.3	500	1.0	103
August 9	pit 4	8.3	500	1.0	106
August 19	pit 4	4.2	500	2.0	168
August 24	pit 4	16.7	500	0.5	110

^a The rate of rainfall application was determined by dividing the volume of water by the time of application and the wetted soil area (6 m^2).

Sample Collection. Before each simulation, the collection bottles were emptied. After rainfall commenced, water was collected most frequently from the shallow row of ZTSs by emptying each bottle before switching the pump tubing to the next bottle. Sampling frequency for the two deeper ZTS rows was increased later in the simulations. The first arrival of small volumes of infiltrating water (10–20 mL) was captured in each ZTS; also, all of the water reaching the ZTSs was sampled.

Field Analyses. Sample mass was measured to determine the volume of infiltrating water. The mass of each sample was measured by weighing the sample and bottle, subtracting the average mass of the containers, and converting mass to volume after accounting for the particle concentration. Earthworms were found in about 10 samples and removed before weighing. Turbidity was measured to determine the particle concentration of each sample. The samples were vigorously shaken, poured into glass test tubes, and measured in a Hach Ratio/XR turbidity meter on the 0–2000 NTU scale.

Laboratory Analyses. For samples with turbidities > 2000 NTU, the particle concentration was measured gravimetrically. Samples were sonicated (80 W, 30 s) and shaken (vortex mixer, 5 min) before aliquots were withdrawn from an intermediate depth in the sample bottle and emptied onto weighed glass dishes in an oven at 105°C overnight. The particle concentrations for the samples with turbidities of greater than 2000 NTU ranged from 4.5 to 9.8 g L^{-1} . The error ($\pm 1\sigma$) for this procedure was 8% of the mean value for replicate samples. The particle concentrations of 11 samples with turbidity less than 2000 NTU were also determined gravimetrically to provide a calibration of turbidity (T , NTU) vs particle concentration (C , g L^{-1}). The calibration curve produced the linear regression $C = 0.0023T$ with the intercept set to zero ($R^2 = 0.986$).

Particle size distributions of 103 samples were determined by a light blocking instrument (Particle Sizing Systems Model 770). The instrument was calibrated using latex beads (1–30 μm). The samples were sonicated and shaken to ensure that the size distribution of primary (disaggregated) particles was measured. Sample dilutions were made with deionized, filtered water. Particle size distributions were reported in 64 channels spanning the size range from 1.0 to 220 μm diameter.

Particles from nine samples were analyzed by scanning electron microscopy (SEM; ISI SX-30) and energy-dispersive X-ray (EDX; Kevex Delta Pro) spectroscopy at 30 kV accelerating voltage. The particles were trapped on 0.22- μm silver filters by suction filtration, attached to aluminum stubs using graphite, and coated with gold.

The electrophoretic mobility of five particle suspensions was measured by laser Doppler velocimetry (Brookhaven ZetaPlus). The samplers were sonicated, shaken, and subsampled as described above and diluted, if necessary, to

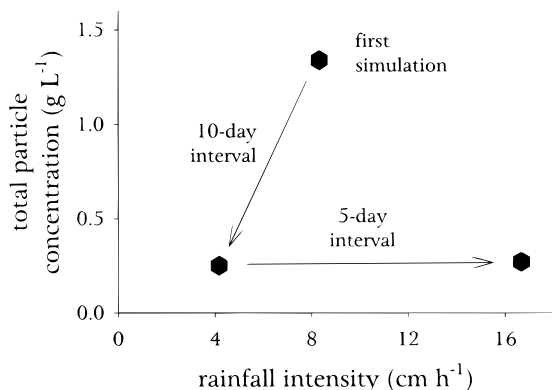


FIGURE 3. Total particle concentrations for all ZTSs versus rainfall intensity during the three simulations for different rainfall intensity in pit 4. Time intervals and order of simulations shown.

obtain the optimal photon count rate. A significant amount of particles settled out of the suspension during measurement. The pH of the particle suspensions was adjusted from 2 to 7 by adding dilute HNO_3 . Each sample was measured in triplicate with a maximum error in the electrophoretic mobility of 30% near the isoelectric point (pH_{iep}).

The ^{238}Pu and $^{239,240}\text{Pu}$ activity of 30 samples was determined by alpha spectroscopy. The samples and an added ^{242}Pu tracer were digested with HF and HNO_3 , reduced to residues, redissolved in HNO_3 , and transferred to an anion exchange resin column (AG 1×8 resin, 100–200 mesh, Cl-form, Bio-Rad Laboratories) converted to nitrate form. Plutonium was eluted from the column by a 1.5 N HCl/0.6% H_2O_2 solution (Pu). The Pu eluents were coprecipitated on NdF_3 and mounted on 0.2- μm membrane filters on carbon/ NdF_3 substrates. Alpha emissions of the samples were counted for 120 min in an EG&G Alpha Eight spectroscopy system. Average yield was $78 \pm 13\%$ for the ^{242}Pu tracer. Control spikes and matrix duplicate spikes prepared by adding ^{238}Pu to a reagent blank and a split of one sample showed accuracies of $99 \pm 10\%$ and $92.8 \pm 9.2\%$, respectively.

Results

Infiltration Rates and Particle Concentrations. Flow into most ZTSs was initially slow, followed by fast and steady flow for a time approximately equal to the rainfall duration. Finally, the fast infiltration was followed by a short period of low flow as the remaining free-flowing water drained into the ZTSs (Supporting Information). A total of 8.3 cm of rainfall was applied in each simulation and the volume flux (cm; total volume of water divided by ZTS area) arriving in the ZTSs ranged from near 0 to 4.6 cm. The total volume and total particle mass arriving in each ZTS during the 8.3 cm h^{-1} simulations in pits 2–4 are shown in Figure 2.

Particle concentrations in the ZTS samples ranged from 0.02 to 9.8 mg cm^{-3} . Particle concentrations were high in the first few samples in most ZTSs and low in the later samples. Total particle concentrations measured during the 4.2 and 16.7 cm h^{-1} events in pit 4 were lower than those measured during the 8.3 cm h^{-1} event (Figure 3). The mean ($\pm\sigma$) total particle concentrations were $1.22 \pm 0.89 \text{ mg cm}^{-3}$ for the 0–20 cm deep ZTSs, $0.51 \pm 0.51 \text{ mg cm}^{-3}$ for the 20–40 cm deep ZTSs, and $2.59 \pm 3.59 \text{ mg cm}^{-3}$ for the 40–70 cm deep ZTSs during the 8.3 cm h^{-1} simulations. The deep ZTSs usually received high concentrations of particles in small volumes of infiltrating water.

Particle Size Distributions. The number of particles decreased with increasing particle size (Figure 4). In duplicate samples, the total number of particles and the number of particles in any size bin varied by less than 10%. The slope of logarithmic plots of particle number per size range ($dN/d\ln d_p$) versus particle diameter (d_p) was used to determine the value of the fitting constant β in the relationship

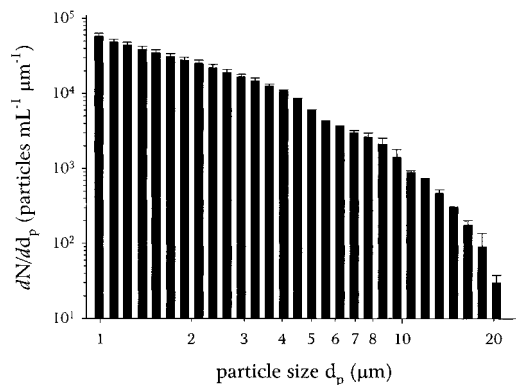


FIGURE 4. Particle size distribution for a single sample, ZTS 4–15, 34 min, 8.3 cm h^{-1} rainfall simulation. Error bars indicate range of duplicate samples.

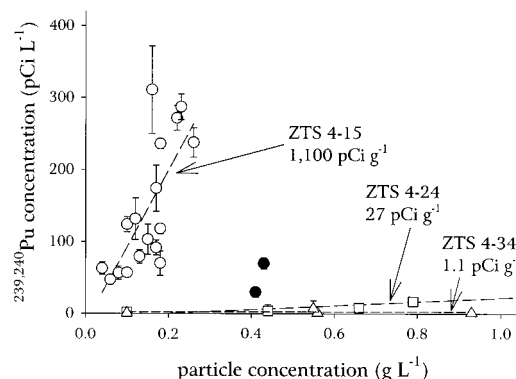


FIGURE 5. $^{239,240}\text{Pu}$ activity versus particle concentration for samples from pit 4 during the 8.3 cm h^{-1} rainfall simulation. Two outliers from ZTS 4–15 (filled circles) are shown on plot but not included in the regression for ZTS 4–15.

$dN/d\ln d_p$, particles $\text{cm}^{-3} \mu\text{m}^{-1}$) versus particle diameter (d_p) was used to determine the value of the fitting constant β in the relationship

$$N = k d_p^{-\beta} \quad (2)$$

in which k is a fitting constant (18). The mean β value for all 103 samples was 2.10 ± 0.09 ($\pm 1\sigma$), indicating that the particle size distributions were quite similar in all of the pits, at all of the depths, and over all of the sampling times.

Particle Morphology, Composition, and Electrophoretic Mobility. The particles consisted of platy fragments in the $<10 \mu\text{m}$ size range and a few larger grains in the 10–50 μm size range. Using an EDX data classification scheme (19), the platy fragments were identified as montmorillonite and the grains as quartz and microcline. Iron peaks in the EDX spectra may reflect the presence of the ferric oxyhydroxide phases responsible for much of the adsorption of plutonium in these sediments (20). The pH_{iep} of the particles were uniformly in the range of 3.0–4.0, consistent with measured pH_{iep} values for 2:1 clay minerals (21).

Plutonium Activity. The plutonium activity of water arriving in ZTSs 15, 24, and 34 decreased with depth with the exception of two outliers of very high Pu or particle concentrations. The total $^{239,240}\text{Pu}$ activity was closely related to particle concentration (Figure 5). The total ^{238}Pu activity was below the detection limit in all but one sample. One sample collected in ZTS 15 during the 4.2 cm h^{-1} simulation registered 1060 pCi L^{-1} , about five times greater $^{239,240}\text{Pu}$ activity than any other sample measured, suggesting that the sample may have contained a pure PuO_2 particle similar to those found at the site in previous surveys (22).

Discussion

Indications of Macropore Flow. The rapid arrival of infiltrating water, the abrupt end of its flow, and the lack of correlation between the volume flux of infiltrating water and the hydraulic conductivity of the soil horizons signaled to Litaor et al. (16) that macropores were the predominant flow path in these soils during similar rainfall simulations in these soils. During our simulations, the arrival of infiltrating water in the ZTSs was even more rapid. The mean and standard deviation of the volume fluxes to all ZTSs was 1.09 ± 0.78 cm during the 1-h 8.3 cm h^{-1} events, about twice the mean volume fluxes ($0.55\text{--}0.62$ cm) measured during their simulations of 100-year return events (7.7 cm h^{-1}) lasting 0.5, 1.0, and 2.0 h. The arrival of infiltrating water usually ended within 30 min after the end of the rainfall application during our simulations, indicating free-flowing water. We also observed a similar lack of correlation between volume flux and hydraulic conductivity of the soil horizons in which the ZTSs were located for the 8.3 cm h^{-1} simulations in pits 2–4 ($R^2 = 0.080$; $n = 38$). From these results, we conclude that the macropores were hydrologically active to depths of at least 70 cm below the surface (the depth of the deepest ZTSs).

Particle Concentration and Infiltration Velocity. We examined the data for correlations between particle concentration and discharge rate, the Darcy velocity of the infiltrating water, calculated as the ratio of the flow rate ($\text{cm}^3 \text{ min}^{-1}$) to the area of the ZTSs (540 cm^2) (Table 3). These discharge rates should be directly proportional to pore velocities; hence, the shear force generated by the infiltrating flow should be directly proportional to these discharge rates. No correlations were observed for the entire data set or for any subset of the data (maximum R^2 of 0.027). The lack of correlation seemed to be the result of the mobilization of high particle concentrations early in the simulations when the instantaneous discharge rates were low ($<0.01 \text{ cm min}^{-1}$).

If the initial pulse of infiltrating water was responsible for mobilization of high particle concentrations, we would expect an inverse relationship between the total particle concentration (the total mass of particles divided by the total volume of water) and total volume of infiltrating water reaching each ZTS (Table 3). These parameters were only weakly correlated at best (maximum R^2 of 0.15), but the slopes were negative for all rainfall simulations. Thus, particle concentrations were generally higher if only small volumes of water reached the ZTSs.

Particle Concentration and Rainfall Intensity. On the basis of shear theory, we expected that particle mobilization would increase with increasing rainfall intensity. The 8.3 cm h^{-1} simulation mobilized more particles than the 4.2 cm h^{-1} simulation; however, the 16.7 cm h^{-1} simulation mobilized fewer particles than the 4.2 cm h^{-1} simulation (Figure 3). We surmise that the 5-day interval between 4.2 and 16.7 cm h^{-1} simulations was insufficient to allow regeneration of the supply of particles in the soil, which places in doubt the difference in particle mobilization observed between the 8.3 and 4.2 cm h^{-1} simulations with a 10-day interval. These tests indicate that processes that generate particles in soils (e.g., aeolian deposition, earthworm burrowing, soil drying, raindrop impact) occur slowly relative to the 5–10-day intervals between these simulations.

Particle Size and Infiltration Velocity. According to shear theory, larger particles will be mobilized by flows of lower velocity, and smaller particles require flows of higher velocity for mobilization. Because discharge rates were initially low and later increased during the simulations, we expected to see larger particles in the initial samples and smaller particles in the later samples. Instead, the particle size distributions in all of the samples measured had a consistent β value (2.10 ± 0.09), indicating that particle size was not related to discharge rate (Figure 6).

TABLE 3. Correlations of Particle Concentration to Instantaneous Discharge Rate (for Each Sample) and Total Particle Concentration to Total Volume of Water (for Each ZTS)

correlation	pit	rainfall rate (cm h^{-1})	slope $\pm \sigma$	intercept $\pm \sigma$	R^2	no.
particle concn (mg cm^{-3}) versus instantaneous discharge rate (cm min^{-1})	2	8.3	-13 ± 31	1.2 ± 0.8	0.012	64 samples
	3	8.3	-15 ± 24	1.2 ± 0.4	0.026	103 samples
	4	8.3	-15 ± 57	1.3 ± 0.9	0.0071	106 samples
	4	4.2	-3.1 ± 6.4	0.28 ± 0.24	0.027	168 samples
total particle concn (mg cm^{-3}) versus total vol of infiltrating water (cm^3)	4	16.7	0.41 ± 2.2	0.24 ± 0.14	0.0048	110 samples
	2	8.3	-0.0028 ± 0.0030	3.3 ± 1.7	0.14	9 ZTSs
	3	8.3	-0.0033 ± 0.0030	0.99 ± 0.28	0.090	14 ZTSs
	4	8.3	-0.0021 ± 0.0030	2.6 ± 1.3	0.035	15 ZTSs
	4	4.2	$-7.5 \times 10^{-5} \pm 8.6 \times 10^{-5}$	0.32 ± 0.09	0.056	15 ZTSs
	4	16.7	-0.00053 ± 0.00035	0.94 ± 0.36	0.15	15 ZTSs

TABLE 4. Correlations of Total Particle Concentration to Soil Properties (Table 2) for Each ZTS ($n = 38$) during the 8.3 cm h^{-1} Simulations in Pits 2–4

total particle concn (mg cm^{-3}) versus	ranges of depth-averaged soil parameters	slope ($\pm\sigma$)	intercept ($\pm\sigma$)	R^2
clay (%)	15.6–32.1	0.17 ± 0.06	-2.1 ± 1.3	0.18
silt (%)	15.6–21.1	0.37 ± 0.22	-5.4 ± 4.1	0.072
sesquioxide (mmol kg^{-1})	82–141	0.014 ± 0.020	-0.068 ± 2.2	0.013
CaCO_3 (mmol kg^{-1})	26–100	-0.027 ± 0.014	3.1 ± 0.91	0.095
CEC ^a (mmol kg^{-1})	226–279	-0.025 ± 0.020	7.9 ± 5.0	0.044
organic carbon (g kg^{-1})	39–160	-0.015 ± 0.011	2.9 ± 1.1	0.055

^a Cation exchange capacity.

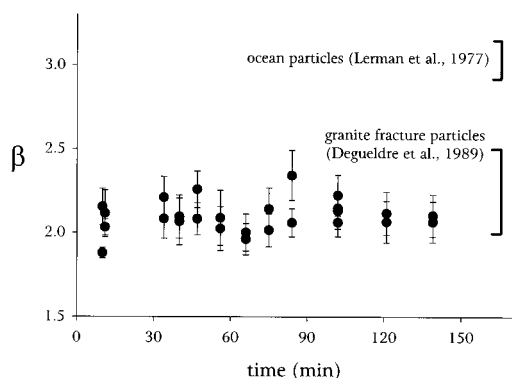


FIGURE 6. Particle size parameter β versus time of rainfall simulations. β is the exponential fitting constant in the relationship relating particle number to particle size, $N = kd_p^{-\beta}$, determined from particle size distributions for samples from ZTS 4–15 during the 8.3 cm h^{-1} simulation. Range of β values reported for particles in oceans and granite fractures shown by brackets on right.

Even though the size of the mobilized particles did not vary with discharge rate, the β values for these particle size distributions suggest that shear may be involved in their generation. Particle size distributions characterized by $\beta \approx 3$, such as those commonly detected in samples from oceans (18), contain equal mass over the range of sizes measured. Size distributions with β values less than 3 have more mass in the larger sizes than in the smaller sizes. Larger particles are preferentially generated by shear or “erosion”. For example, Degueldre et al. (23) measured β values between 2.0 and 2.5 for particle size distributions in samples collected from granite fractures through water flowed freely.

The particle size distribution results reported here cannot be compared directly to those reported by Kaplan et al. (4). We examined particle greater than $1 \mu\text{m}$ using a light-blocking technique that, like electrical conductivity (e.g., the Coulter Counter) and direct particle counting (optical and electron microscopy) techniques, typically reports particle size distributions that conform to the power law $N = kd_p^{-\beta}$. They focused on particles less than $1 \mu\text{m}$ using photon correlation spectroscopy, a technique that is best suited to measurement of monodisperse particle distributions (24).

Particle Concentration and Soil Composition. We examined the correlation of total particle concentrations in the three soil pits with properties of the soil horizons in which the ZTSs were located (Table 4). For deeper ZTSs, the soil properties of the overlying horizons was depth-averaged to reflect the flow path from the surface to the ZTSs. A very weak correlation was observed for the clay content of the soils (R^2 of 0.18), which may suggest that the clay-sized fraction is a source of particles, but this correlation was largely influenced by just a few samples from deep ZTSs in high clay horizons that received little water and, thus, high total particle concentrations. No correlations better than R^2 of 0.095 were

detected between total particle concentration and other soil properties.

Interestingly, particle concentration was not related to the sesquioxide content of the soil horizons, despite the important role of positively charged oxides in limiting the transport and controlling the mobilization of particles (25, 26), nor was particle concentration related to the organic carbon content of the soil horizons, even though organic matter adsorption can strongly influence the particle–grain interactions that control particle mobilization (4, 27). The lack of correlations may be attributed to the relatively small range of soil properties in these soils.

Plutonium Transport during Rainfall Simulations. The correlation between total $^{239,240}\text{Pu}$ activity and particle concentration (Figure 5) reinforce the assumption that plutonium transport is dominated by particles. Recently, Litaor et al. (14) showed that 83–97% of the actinides present in the interstitial waters of the Rocky Flats soils were associated with particles trapped on $0.45\text{-}\mu\text{m}$ filters. The distribution of plutonium with depth closely matched the plutonium distributions measured by Litaor et al. (15, 16) in the soils and infiltrating water.

The activity of $^{239,240}\text{Pu}$ in the infiltrating water decreases by 3 orders of magnitude from the shallowest to deepest ZTS in Pit 4 (Figure 5), indicating that the transport of plutonium by infiltrating rainfall is substantially attenuated in the upper soil horizons. Using plutonium as a tracer of the particle transport, we infer that most of the particles arriving in the deeper ZTSs must have been mobilized near those ZTSs and not transported from the upper horizons.

Possible Effects of Macropores on Particle and Plutonium Transport. The lack of correlations between particle concentration, particle size, infiltration velocity, and soil type may be caused by the dominance of macropore flow in these soils. For example, if most of the infiltration in the Rocky Flats soils was funneled through macropores, the supply of particles may have been quickly exhausted by the initial pulses of infiltrating water, resulting in a lack of correlation between particle concentration and discharge rate. Our results differ from those of Kaplan et al. (4), who observed a strong correlation between particle concentration and infiltration flow rate in a soil that was repacked into a test chamber, which likely resulted in the loss of any macroporosity or preferential flow paths. On the other hand, Biddle et al. (5) did not observe any correlation between particle concentration and rainfall intensity in natural, undisturbed soils in which macropore structure may have been preserved.

The lack of correlation between particle concentration and soil properties may also be caused by flow through macropores. If the composition of the macropore linings are different from that of the surrounding bulk soil as other researchers have observed (28), any relationship between the bulk soil properties and particle concentration may be obscured. For these Rocky Flats soils, we know only that the plutonium activity of the macropore fillings was significantly

greater than in the surrounding soils (15). The constancy of particle size with varying infiltration velocities may also be caused by macropores. Earthworm burrowing that produced the macropores may also produce an abundance of reworked soil particles of relatively uniform size in the macropores. Owing to prohibition of the removal of contaminated soil from the site, we could not obtain samples from the pits to confirm these hypotheses. Further experiments are necessary to provide environmental managers with better predictive tools for assessing the effects of rainfall intensity on particle and particle-associated contaminants in soils.

Acknowledgments

We acknowledge the support of the U.S. Department of Energy, EG&G Rocky Flats, and the National Science Foundation (Grant CTS-9410301); Keith Ethridge, Tom Temple, Bob Snyder, Bob Lahn (Woodward-Clyde), Gil Barth, Hans Daniels (EG&G Rocky Flats), Elizabeth Zika (U.S. DOE), Terrence Biever, Blair Greimann (University of Colorado), and John Holmes (University of Missouri) for assistance in the field; Patrick Siebert (University of Colorado) for the particle concentration and size analyses; Dave Nicoli (Particle Sizing Systems, Inc.) and Ken Crowe (Southwestern Engineering and Equipment Co.) for use of the Particle Sizing Systems 770; John Drexler (University of Colorado) for SEM/EDX analysis; and Robert Murphy (Colorado School of Mines) for assistance with the plutonium analysis.

Supporting Information Available

Five additional figures plus a caption showing the particle concentrations and cumulative water volume arriving in ZTSs in different places and times (6 pp) will appear following these pages in the microfilm edition of this volume of the journal. Photocopies of the Supporting Information from this paper or microfilm (105 × 148 mm, 24× reduction, negatives) may be obtained from Microforms Office, American Chemical Society, 1155 16th St. NW, Washington, DC 20036. Full bibliographic citation (journal, title of article, names of authors, inclusive pagination, volume number, and issue number) and prepayment, check or money order for \$16.50 for photocopy (\$17.50 foreign) or \$12.00 for microfiche (\$13.00 foreign), are required. Canadian residents should add 7% GST. Supporting Information is also available via the World Wide Web at URL <http://www.chemcenter.org>. Users should select Electronic Publications and then Environmental Science and Technology under Electronic Editions. Detailed instructions for using this service, along with a description of the file formats, are available at this site. To download the Supporting Information, enter the journal subscription number from your mailing label. For additional information on electronic access, send electronic mail to si-help@acs.org or phone (202)872-6333.

Literature Cited

- (1) Vinten, A. J. A.; Yaron, B.; Nye P. H. *J. Agric. Food Chem.* **1983**, *31*, 662.

- (2) Amrhein, C.; Mosher, P. A.; Strong J. E. *Soil Sci. Soc. Am. J.* **1993**, *57*, 1212.
- (3) Pilgrim, D. H.; Huff, D. D. *Earth Surf. Proc. Landforms* **1983**, *8*, 451.
- (4) Kaplan, D. I.; Bertsch, P. M.; Adriano, D. C.; Miller, W. P. *Environ. Sci. Technol.* **1993**, *27*, 1193.
- (5) Biddle, D. L.; Chittleborough D. J.; Fitzpatrick, R. W. *Appl. Clay Sci.* **1995**, *9*, 433.
- (6) Walker, T. R.; Waugh, B.; Grone, A. J. *Geol. Soc. Am. Bull.* **1978**, *89*, 19.
- (7) McKeague, J. A.; Guertin, R. K.; Valentine, K. W. G.; Bélisle, J.; Bourbeau, G. A.; Howell, A.; Michalyna, W.; Hopkins, L.; Pagé, F.; Bresson, L. M. *Soil Sci.* **1980**, *129*, 386.
- (8) Ryan, J. N.; Elimelech, M. *Colloids Surf. A: Physicochem. Eng. Aspects* **1996**, *107*, 1.
- (9) O'Neill, M. E. *Chem. Eng. Sci.* **1968**, *23*, 1293.
- (10) Sharma, M. M.; Chamoun, H.; Sita Rama Sarma, D. S. H.; Schechter, R. S. *J. Colloid Interface Sci.* **1992**, *149*, 121.
- (11) Thomas, G. W.; Phillips, R. E. *J. Environ. Qual.* **1979**, *8*, 149.
- (12) Smith, M. S.; Thomas, G. W.; White, R. E.; Ritonga, D. *J. Environ. Qual.* **1985**, *14*, 87.
- (13) Goss, D. W.; Smith, S. J.; Stewart, B. A.; Jones, O. R. *Water Resour. Res.* **1973**, *9*, 668.
- (14) Litaor, M. I.; Barth, G. R.; Zika, E. M.; Litus, G.; Moffitt, J.; Daniels, H. *J. Environ. Radioact.* In press.
- (15) Litaor, M. I.; Thompson, M. L.; Barth, G. R.; Molzer, P. C. *J. Environ. Qual.* **1994**, *23*, 1231.
- (16) Litaor, M. I.; Barth, G. R.; Zika, E. M. *J. Environ. Qual.* **1996**, *25*, 671.
- (17) Seed, J. R.; Calkins, K. W.; Illsley, C. T.; Miner, F. J.; Owen, J. W. *Committee Evaluation of Pu Levels in Soils Within and Surrounding USAEC Installation at Rocky Flats, Colorado*; Report RFP-INV-1; Dow Chemical Co.: Golden, CO, 1971.
- (18) Lerman, A.; Carder, K. L.; Betzer, P. R. *Earth Planet. Sci. Lett.* **1977**, *37*, 61.
- (19) Mudroch, A.; Zeman, A. J.; Sandilands, R. *J. Sed. Petrol.* **1977**, *47*, 244.
- (20) Litaor, M. I.; Imbrahim, S. A. *J. Environ. Qual.* **1996**, *25*, 1144.
- (21) Parks, G. A. In *Equilibrium Concepts in Natural Water Systems*; Stumm, W., Ed.; ACS Symposium Series 67; American Chemical Society: Washington, DC, 1967; pp 121–160.
- (22) McDowell, L. M.; Whicker, F. W. *Health Phys.* **1978**, *35*, 293.
- (23) Degeldre, C.; Baeyens, B.; Goerlich, W.; Riga, J.; Verbist, J.; Stadelmann, P. *Geochim. Cosmochim. Acta* **1989**, *53*, 603.
- (24) Rees, T. F. *Water Resour. Res.* **1990**, *26*, 2777.
- (25) Harris, W. G.; Carlisle, V. W.; Chesser, S. L. *Soil Sci. Soc. Am. J.* **1987**, *51*, 1673.
- (26) Ryan, J. N.; Gschwend, P. M. *Geochim. Cosmochim. Acta* **1992**, *56*, 1507.
- (27) Ryan, J. N.; Gschwend, P. M. *Environ. Sci. Technol.* **1994**, *28*, 1717.
- (28) Stehouwer, R. C.; Dick, W. A.; Traina, S. J. *J. Environ. Qual.* **1993**, *22*, 181.

Received for review April 15, 1997. Revised manuscript received November 12, 1997. Accepted November 21, 1997.

ES970339U